LA-UR- 11-02787

Approved for public release;
distribution is unlimited.

Title:	Plasma Sprayed Zirconium Thermal Diffusion Behavior
Author(s):	Kendall J. Hollis
Intended for:	Proceedings of the 2011 International Thermal Spray Conference, Hamburg, Germany, Sept. 27-29, 2011

Form 836 (7/06)

Plasma Sprayed Zirconium Thermal Diffusion Behavior

Kendall J. Hollis, Los Alamos, NM / USA

International Thermal Spray Conference, September 27-29, 2011, Hamburg, Germany

Zirconium (Zr) metal is of interest for chemical corrosion protection and nuclear reactor core applications. Inert chamber plasma spraying has been used to produce thin Zr coatings on stainless steel (SS) substrates. The coatings were deposited while using transferred arc (TA) cleaning/heating at 5 different current levels. In order to better understand thermal diffusion governed processes, the coating porosity, grain size and interdiffusion with the substrate were measured as a function of TA current. Low porosity (3.5% to <0.5%), recrystallization with fine equiaxed grain size (3-8 μm diameter) and varying elemental diffusion distance (0-50 μm) from the coating-substrate interface were observed. In addition, the coatings were low in oxygen content compared to the wrought SS substrates. The Zr coatings sprayed under these conditions look promising for highly demanding applications.

1 Introduction

Zirconium (Zr) metal exhibits excellent resistance to corrosive attack in most organic and inorganic acids, salt solutions, strong alkalis and some molten salts [1]. Zr is also well suited to use in nuclear reactors due to its low thermal neutron absorption cross section, good mechanical strength and relatively high melting temperature (1855°C). A possible use for Zr coatings is steel shells lined with Zr for use in chemical reactor vessels and piping. Another use for Zr coatings is as a diffusion barrier between low enriched uranium and aluminum for use in high performance research reactor fuel [2]. In both cases, low porosity and good adhesion between the coating and substrate are of high importance.

Very little information on the properties of plasma sprayed zirconium is available in the literature [3]. The goal of this study is to investigate techniques for producing high quality Zr coatings and explore the thermal diffusion governed properties of sintering, grain growth and interface diffusion of the coatings.

2 Experimental procedure

The samples used for this study were 304 stainless steel (SS) with size 32 mm x 102 mm x 0.25 mm. The Zr powder used was 99.2% minimum purity Zr (ATI Wah Chang, Albany, OR, USA) with particle sizes between 50 μm and 5 μm. Thin (40-70 μm) coatings were sprayed in a controlled atmosphere chamber (filled with argon and maintained at 47kPa) using an SG-100 plasma torch (Praxair/TAFA, Concord, NH, USA) operating at 850 A and 26 V with 40 slm Ar, 15 slm He, 3 slm Ar powder gas, powder flowing at 8 g/min and a torch to substrate distance of 100 mm. Both sides of the substrate were coated on subsequent spray runs. Before, during and after deposition, a transferred arc (TA) between the torch face and the substrate was utilized for cathodic arc cleaning and substrate heating. The TA power supply was configured to produce alternating square-wave current (40, 50, 60, 70, or 80 A) at 100 Hz with equal duration on the positive and negative cycles. TA cleaning and heating were performed for two torch passes without powder feed followed by eight torch passes with powder feed. Two additional cleaning and heating torch passes immediately followed the coating process for most samples. Side 2 of the 70 A TA coating and side 1 of the 80 A TA coating had 4 post deposition passes and side 2 of the 80 A TA coating had 8 post deposition passes. The additional passes on the second coated side were performed in an attempt to equilibrate the time-temperature thermal processing histories of the two sides of the same sample. The temperature of the substrate was monitored by a K type (chromel/alumel) thermocouple in contact with the back side of the substrate throughout the spray run.

Coated samples were cross sectioned, mounted, ground and polished for observation. Volumetric porosity of the samples was estimated by measuring the area of porosity within the cross sectional light optical microscope (LOM) images in the as-polished condition. No oxides were observed in the cross sections making the thresholding operation to differentiate between the Zr coating and porosity more straightforward. For each coating, eight images from random locations in the cross section were chosen and the average pore area for each coating was calculated. The as polished samples were also imaged using an SEM in back scatter electron (BSE) mode and energy dispersive spectroscopy (EDS) elemental maps were generated of coating cross sections. In addition, atomic force microscopy (AFM) and Kelvin force probe microscopy (KFPM) (Dimension 3100, Bruker AXS Inc., Santa Barbara, CA, USA) were used to investigate sample cross sections for topography and work function mapping respectively. Samples were then etched to better reveal the grain structure. LOM images were taken of the etched samples under polarized lighting. Grain size analysis was performed according to ASTM E112-10 using the Abrams three-circle intercept procedure.

3 Results

3.1 Substrate temperature

The substrate temperature increased throughout the run and the peak temperatures for each run are shown in **Fig. 1**. The higher temperatures for side 2 compared to side 1 at 70 A and 80 A TA are due to the additional post deposition passes on side 2. The amount of time at high temperature for the coating on side 1 is at least twice the time for the coating on side 2 since the side 1 coating is also heated up during the coating of side 2.

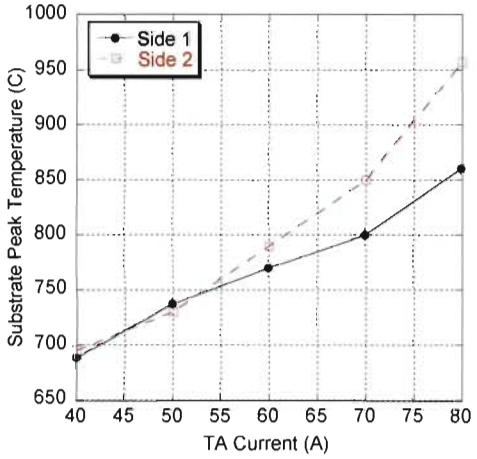

Fig. 1. Peak substrate temperature versus TA current.

3.2 Porosity

The average porosity for each coating is shown in **Fig. 2** with the error bars correspond to one standard deviation of all measured values from the mean. Since the coatings showed some systematic variation in porosity (higher at the sample edges and lower in the center) the standard deviation at a given location is smaller than the error bars shown in the figure. The figure shows that the porosity decreases as the TA current increases. In addition, the coating on side 1 contains less porosity than the coating on side 2 for all samples. At 80 A TA, the side 1 and side 2 coatings are very nearly fully dense.

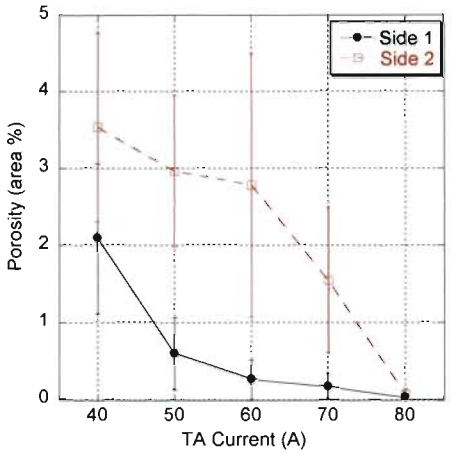

Fig. 2. Zr coating porosity versus TA current.

3.3 Grain size

Polarized light LOM cross sectional views of etched Zr coating samples are shown in **Fig. 3 a-e**. The coating grains are primarily equiaxed in morphology without evidence of the individual flattened powder particles which compose the coating. Coatings sprayed at 40 A TA showed small areas (< 5% area side 1 and < 10% area side 2) that may not have been recrystallized while the other coatings appear to be fully recrystallized. Average grain diameter measurements for each coating are shown in **Fig. 4** with the error bars correspond to one standard deviation of all measured values from the mean. Similar to the porosity measurements above, systematic variation in the grain size with location was observed so the standard deviation at a given location is less than the error bars shown. Grain size increases with increasing TA current with grain size on side 1 exceeding that of side 2 for all samples.

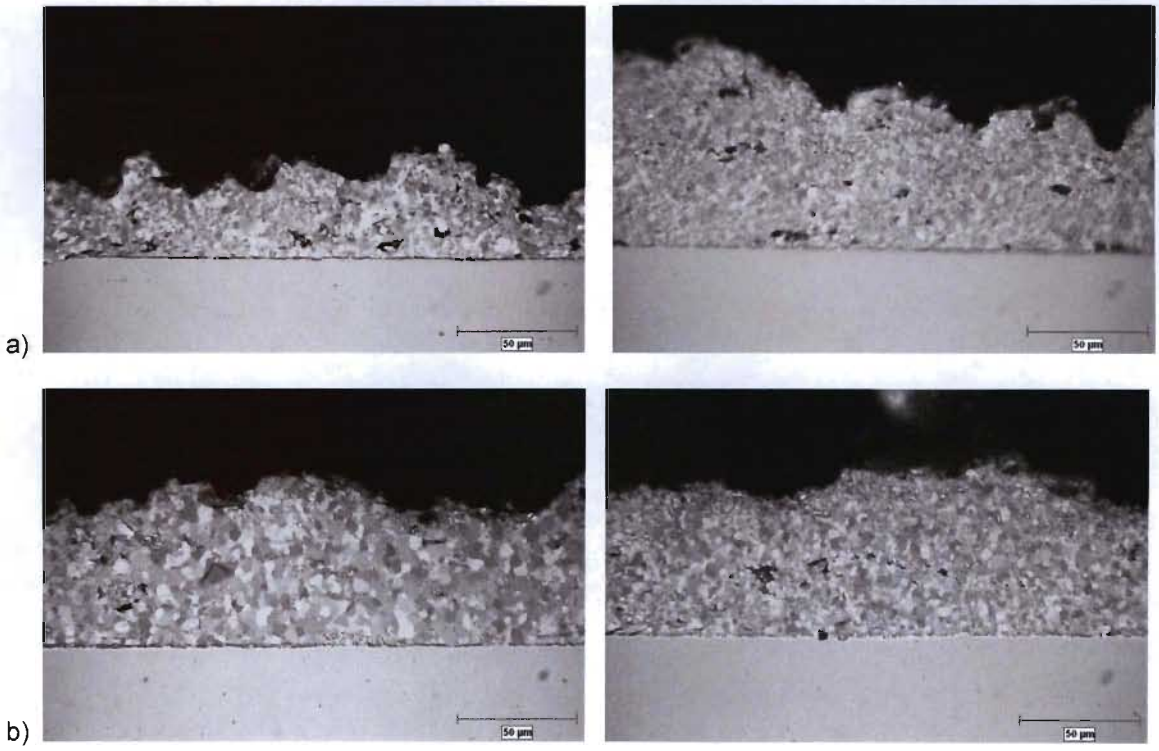

Fig. 3. Polarized LOM images of Zirconium coatings sprayed at 40 a), 50 b), 60 c), 70 d), and 80 e) A TA. The image on the left is the first coating sprayed (side 1) and the image on the right is the second coating sprayed (side 2) on the opposite side of the substrate as the first. The marker size for all images is 50 μm.

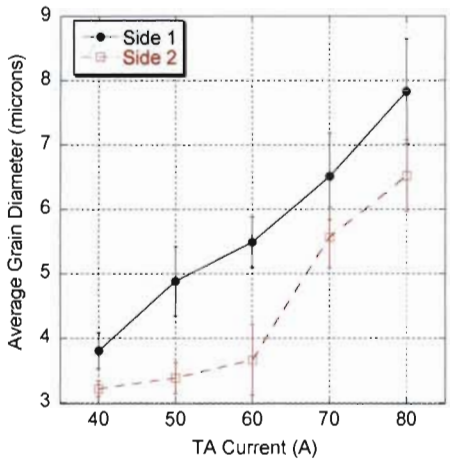

Fig. 4. Zr coating grain diameter versus TA current.

3.4 Diffusion zone

As can be observed in **Fig. 3 e)**, there is a region in the coating next to the substrate with a structure different from the remainder of the coating. A higher magnification image of this region with lighting conditions optimized to show differences in the structure is shown in **Fig. 5**. The region near the substrate has a smaller grain size and a less uniform grain morphology. This band appears to be a diffusion region where elements from the SS substrate diffused into the Zr coating. The maximum thickness of this diffusion band for the various coatings is shown in **Fig. 6**. Similar to porosity and grain size, the band thickness showed systematic variation with location (thinner at the substrate edges and thicker in the center). The band thickness generally increases as TA current increases and is greater for side 1 than side 2. No diffusion band is observed for 40 and 50 A TA and at 80 A TA, the band thicknesses for side 1 and side 2 are similar.

Fig. 5. Polarized light LOM image of an etched Zr coating showing a diffusion zone of thickness 25 μm next to the Zr/SS interface. The marker is 20 μm.

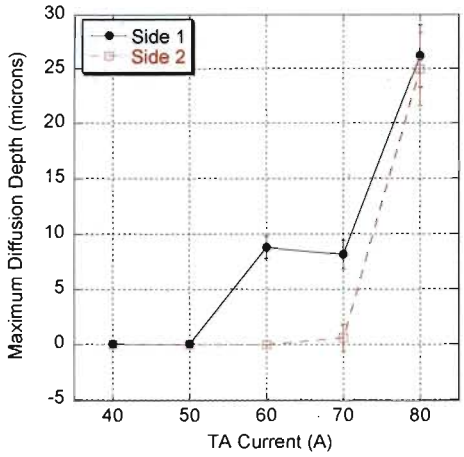

Fig. 6. Maximum diffusion band depth versus TA current.

In order to further investigate the nature of the diffusion band, AFM, KFPM, SEM-BSE and SEM-EDS imaging was performed at the coating-substrate interface. The KFPM and AFM images of samples sprayed using 60 and 80 A TA are shown in **Fig. 7**. The KFPM images are helpful in visualizing regions of varying chemical composition as the work function will vary according the chemical composition. The KFPM image in **Fig. 7 b)** shows the SS at the extreme bottom of the image (darkest phase) abruptly transitioning to the Zr coating above it. No interdiffusion between coating and substrate is observed for side 2 at 60 A TA. The corresponding AFM image in **Fig. 7 b)** does not show a fine grained band at the interface. **Fig. 7 a)** showing side 1 at 60 A TA shows an intermixed region of 7 μm depth in the KFPM image and small grains in a similar band width in the AFM image. The side 2 coating at 80 A TA (**Fig. 7 d)**) shows an intermixed, fine grain sized region of 17 μm thickness. Also evident in the KFMP image of the larger grained coating at the top of the image is a difference in composition between the center of the grains and the grain boundaries. This difference is not observed by the topography in the corresponding AFM image. **Fig. 7 c)** depicting the side 1 coating at 80 A TA, shows a fine grained band of thickness 20 μm in the AFM image and a similar thickness intermixed band in the KFPM image. The Zr coating above the intermixed band shows compositional variation (KFMP) on a scale smaller than the grain size (AFM).

a)

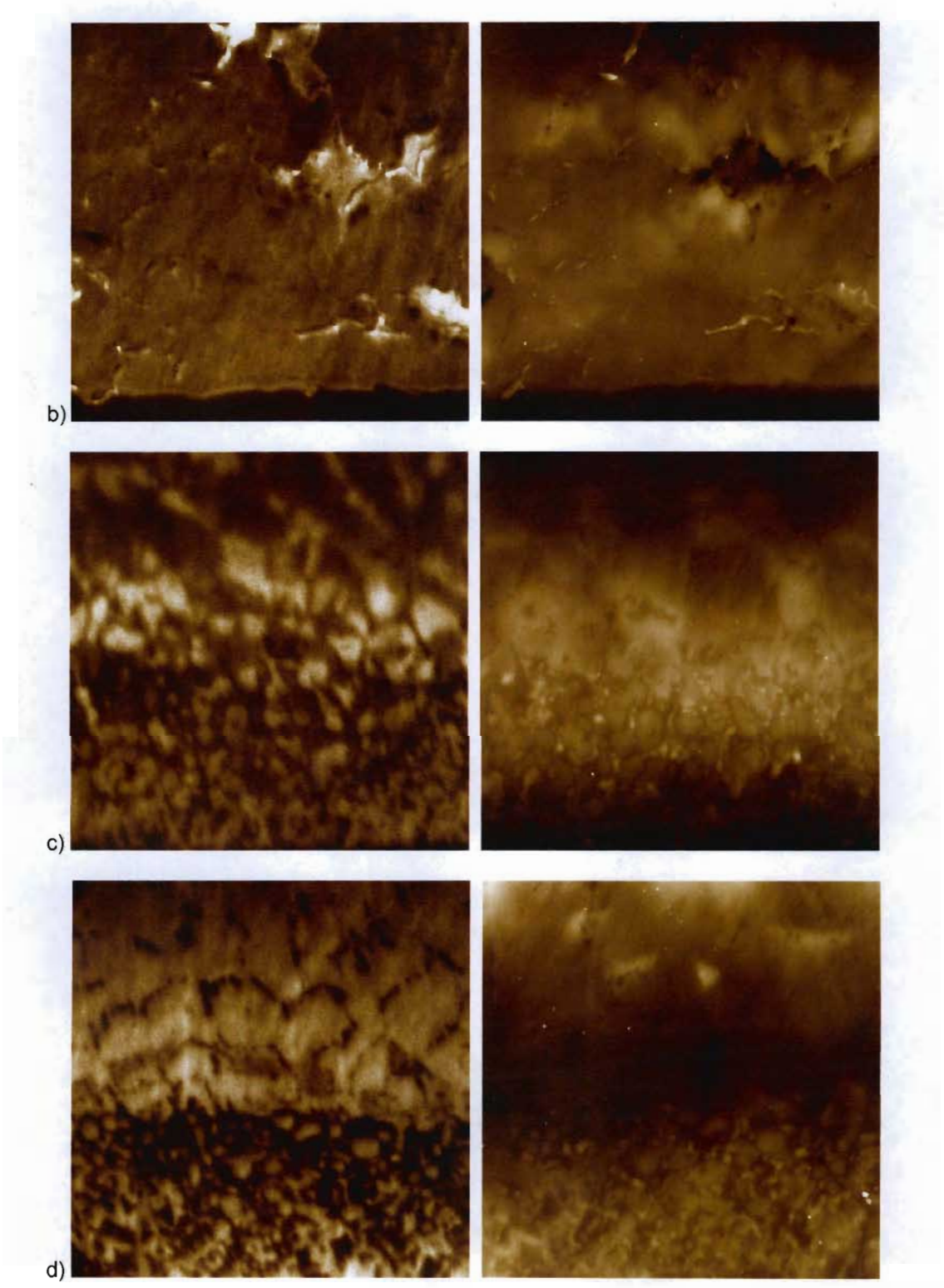

Fig. 7. KFPM images of surface contact potential (a measure of the localized surface work function) (left image) and AFM surface topography (right image) showing the coating-substrate interface with the Zr at the top of the image and the SS at the bottom for a) 60 A TA side 1, b) 60 A TA side 2, c) 80 A TA side 1 and d) 80 A TA side 2. The images are 40 μm on each side and

the full dynamic range (black to white) represents 300 mV for the KFPM images and 250 nm for the AFM images.

The SEM-BSE image and SEM-EDS elemental maps of the Zr-SS interface for side 2 of the 80 A TA sample are shown in **Fig. 8**. Clear interdiffusion between the Zr coating and the SS substrate elements (Fe, Cr, Ni) is evident. The Fe elemental map shows the Fe spread throughout the diffusion band and, in addition, Fe is visible along the Zr grain boundaries to within 15 μm of the top of the Zr coating. The Cr also diffuses into the Zr but does not extend as far as the Fe and fill the diffusion band as completely as the Fe. The Cr is not observed along the grain boundaries of the Zr grains above the diffusion band. There is a line of high Cr concentration just below the diffusion band in the SS. The Ni signal is not as strong as the Fe and Cr but the Ni is seen to diffuse to the top of the diffusion band. Ni is not observed along Zr grain boundaries above the diffusion band. Oxygen is observed in the SS substrate and in the diffusion band but very little is observed within the Zr. The O concentration is high along a line just below the diffusion band in the SS similar to the Cr. Although the O signal is relatively weak, on careful examination of the elemental maps, the O pattern seems to match the Cr pattern better than the Fe pattern.

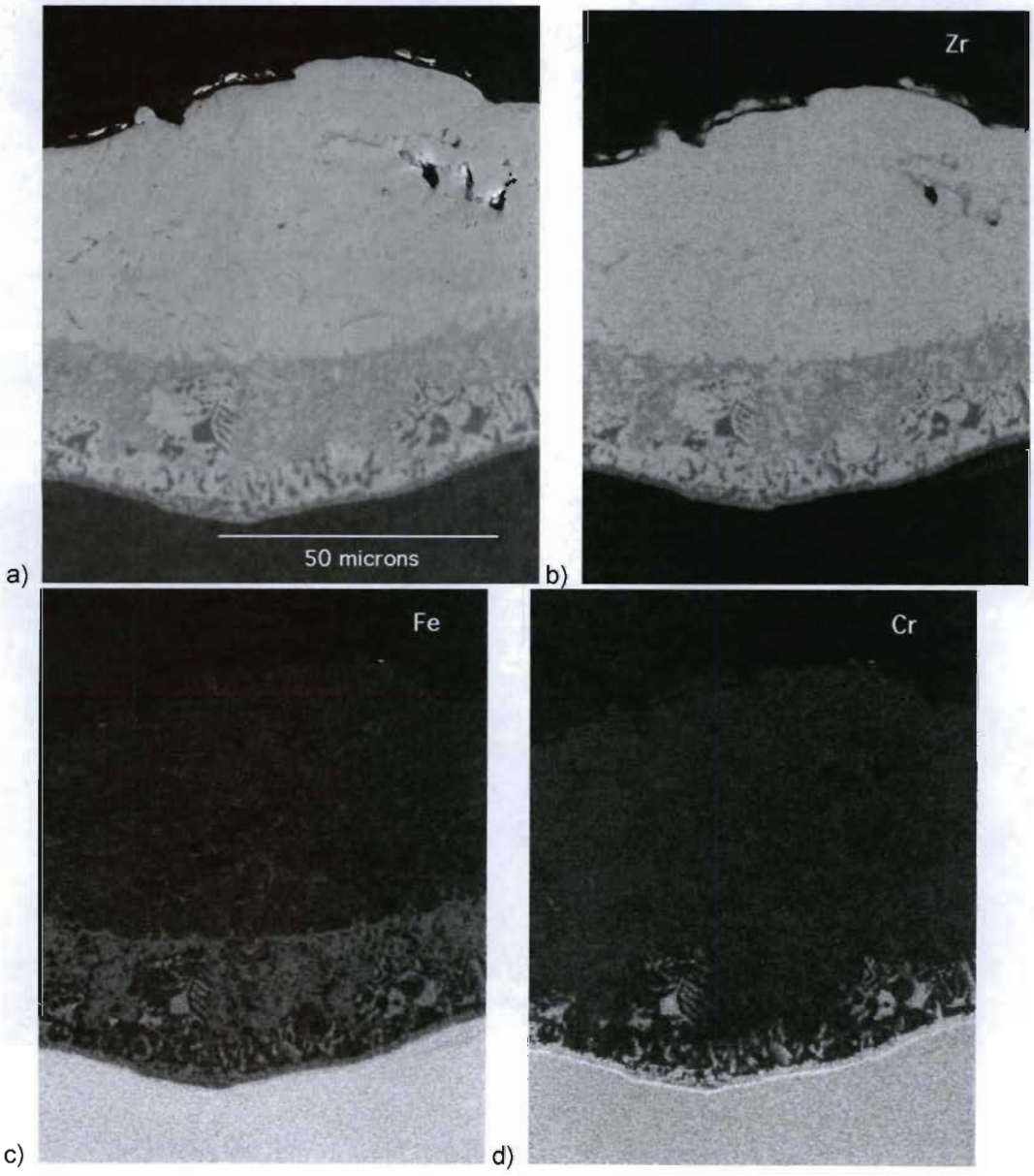

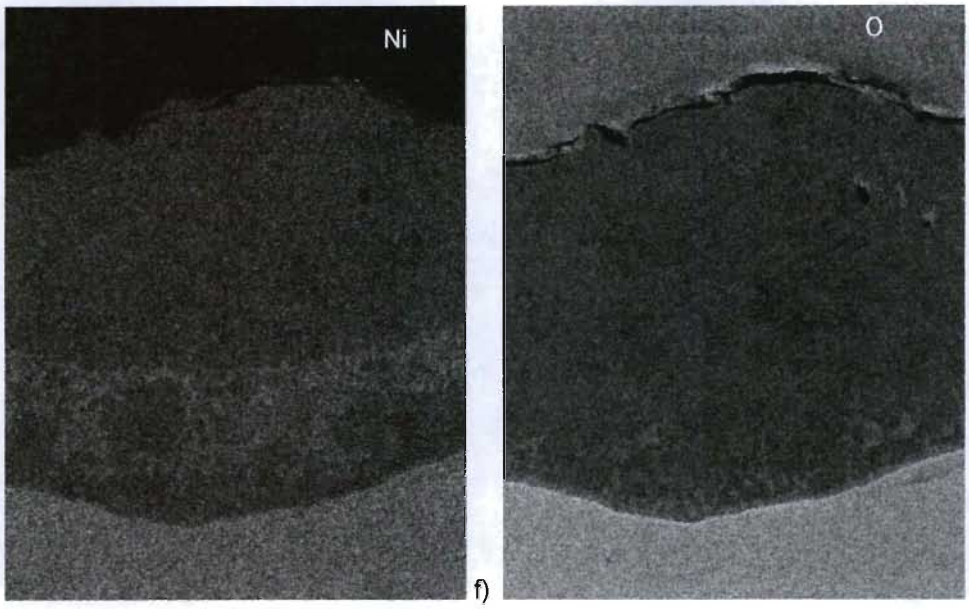

Fig. 8. SEM-BSE image a) and SEM-EDS elemental maps for Zr b), Fe c), Cr d), Ni e) and O f).

4 Discussion

Grain growth, sintering and interface species diffusion are all thermal diffusion governed processes that can be represented by Arrhenius relations such as Eq. 1

$$\kappa = A\, t^{n} \exp(-E_{\alpha}/RT) \qquad (1)$$

where κ is the rate constant for the particular mechanism under consideration, A is the pre-exponential constant, t is time, n is a unitless factor typically in the range $-1<n<1$, E_{α} is the activation energy for the mechanism, R is the universal gas constant and T is the absolute temperature. Diffusion is most significant at temperatures above about 40% of the absolute melting temperature of the material (851K or 578°C for Zr). The extent of diffusion depends on temperature, time, the nature and concentration of diffusing species, the crystal structure and composition of the matrix, stiochiometry, and point defects [5].

Grain growth involves the movement of grain boundaries by diffusion of atoms across the grain boundary to lower the thermodynamic energy by reducing grain boundary area. Sintering is driven by surface area (and consequently surface energy) minimization causing interface bridging, pore spherodization, and a decrease in total porosity. Diffusion occurs more easily along surfaces and voids in the material (like grain boundaries) because fewer atoms need to move to let the diffusing atom pass.

Recrystallization appears to be complete for all samples with 50 A TA and higher. Samples sprayed at 40 A TA were almost completely recrystallized. Treco [6] has shown that complete recrystallization of wrought Zr occurs after 360 seconds at 700°C (5% reduction in area (RA)) to 565°C (95% RA) depending on the extent of cold work. Side 2 of the 40 A TA sample saw the lowest time-temperature excursion with a peak temperature of 690°C and a run duration of 92 seconds while side 1 of the same sample had a total run time (both sides) of 183 seconds. Side 1 and side 2 of the sample sprayed at 50 A TA had a peak temperature of 735°C for 185 sec. and 92 sec. respectively. Since the thermocouple was on the back of the substrate, the coating was slightly higher in temperature than the measurement. The coating is expected to have some residual stress from the quenching of individual particles from their melting temperature to the substrate temperature. This stress could produce some degree of lattice damage similar to cold

working. The observation of complete recrystallization in the samples sprayed at 50A TA and nearly complete recrystallization for the samples sprayed at 40 A TA is consistent with Ref. 5 for wrought Zr with a small amount of cold work.

Grain growth for the Zr coatings appear to be continuous (or normal) with no evidence of a small number of very large grains as characterizes discontinuous (or abnormal) growth. An increase in grain size with both time (side 1 versus side 2) and temperature (as a function of TA current) is consistent with an Arrhenius type thermal diffusion process.

Likewise, porosity of the Zr coatings decreases with time and temperature. In an effort to densify the coatings on side 1 and side 2 to a more similar degree, the number of post deposition passes was increased for side 2 to increase the temperature compared to side 1 for the 70 and 80 A TA coatings. **Fig. 2** shows that this technique was effective with side 2 coatings showing a substantial decrease in porosity from 60 to 80 A TA while side 1 of the same coatings showed only a small decrease in porosity.

Diffusion across the Zr-SS boundary did not occur for side 1 until 60 A TA and for side 2 until 70 A TA. At 80 A TA, the diffusion was significant with Fe diffusing almost all the way through the Zr coating at the Zr grain boundaries. The Ni diffused throughout the diffusion band but could not be observed at the Zr grain boundaries perhaps due to the low intensity of the Ni EDS signal. The Cr, however, diffused mainly into the lower parts of the diffusion band and showed shorter diffusion distances than the Fe and Ni. The diffusion coefficients for Fe, Ni and Cr in Zr at 827°C are 1.5×10^{-10} m^2/s, 8.5×10^{-11} m^2/s and 6×10^{-13} m^2/s respectively [6]. These diffusion coefficients are qualitatively in agreement with the diffusion distances observed for Fe, Ni and Cr in the Zr coatings. The oxygen is primarily co-located with the Cr in the diffusion band indicating that the oxygen is likely in the form of a Cr oxide. There appears to be a higher concentration of O in the wrought SS than in the Zr coating.

The samples produced for this study had substrate temperatures that increased throughout spraying. This increasing temperature is not amenable to calculation of process constants for various mechanisms (activation energy, grain growth exponent, diffusion constants, etc.) which are calculated utilizing data from various times at constant temperature. Therefore, accurate comparison with literature values for process constants is not possible for the samples investigated here.

5 Conclusions

- Plasma sprayed Zr porosity varied with time and substrate temperature in the range from 3.5% to < 0.5%.
- Zr coating recrystallization was complete for samples sprayed with 50 A TA and above showing agreement with wrought Zr recrystallization with a small amount of cold work.
- Zr coating average grain diameter varied with time and substrate temperature in the range of 3-8 μm.
- Diffusion of Fe, Cr and Ni from the substrate into the Zr coating occurred for coatings at the highest times and substrate temperatures.
- High quality Zr as-sprayed coatings with low oxide, fine, equiaxed grain size, high density and diffusion bonding to the substrate are demonstrated with possible applications in nuclear reactors and high corrosion environments.

6 Acknowledgement

The authors would like to acknowledge Ann Kelly, Robert Forsyth and J.D. Montalvo for their help with metallographic preparation and LOM imaging, Pat Dickerson for her help with SEM imaging and Marilyn Hawley for her help with AFM/KFPM imaging. This work was funded by the DOE NNSA Global Threat Reduction Initiative's Reactor Conversion Program.

7 References

[1] http://www.wahchang.com/pages/products/cpi/cpi.htm

[2] K.J. Hollis, "Zirconium Diffusion Barrier Coatings for Uranium Fuel used in Nuclear Reactors", Advanced Materials & Processes (2010) Vol. 168, No. 11, pp. 57/9.

[3] K.J. Hollis, M.I. Pena, "Plasma Sprayed and Electrospark Deposited Zirconium Metal Diffusion Barrier Coatings", Thermal Spray: Global Solutions for Future Application, DVS-ASM, May 2010, pp. 439/44.

[4] R.M. Treco, "Recrystallization and Grain Growth in Iodide Zirconium", J. of Metals, Oct. 1956, pp. 1304-11.

[5] The Science and Engineering of Materials, D.R Askeland, P.P. Phule, Thompson Learning, Toronto, ON, Canada, pp. 174/5.

[6] R.A. Perez, H. Nakajima, F. Dyment, "Diffusion in α-Ti and Zr", Materials Transactions, Vol. 44, No. 1 (2003) pp. 2/13.